Acta Cryst. (1996). A52, 890–897

Profile-Fitting Treatment of Single-Crystal Diffraction Data

A. PAVESE* AND G. ARTIOLI

Dipartimento Scienze della Terra, Sezione Mineralogia, Università degli Studi di Milano, Via Botticelli 23, Milano 20133, Italy. E-mail: pavese@iummi4.terra.unimi.it

(Received 22 January 1996; accepted 12 June 1996)

Abstract

Profile-fitting methods have received great attention in the area of structure analysis from powder diffraction data. Although the use of profile fitting for the reliable extraction of integrated intensities from single-crystal diffraction data has long been proposed in the literature, a limited number of applications and tests of the method have been performed on single-crystal X-ray or neutron diffraction profiles. The profile-fitting technique is here employed to extract integrated intensities from two troublesome data sets of single-crystal diffraction profiles, one affected by multiple scattering effects (X-ray) and the other showing scan truncation (neutrons). It is shown that the proposed implementation of the profile-fitting procedure has great advantages in producing reliable integrated intensities compared with conventional integration methods. Furthermore, during the data processing, any anomalous diffraction profile is easily detected and proper analysis of instrumental background and scan-truncation effects is performed. The method thus allows effective evaluation of the quality of the treated data set. It is proposed that the profile-fitting technique for the extraction of single-crystal integrated intensities be used routinely when diffraction data of superior quality are needed for crystal structure analysis.

1. Introduction

Single-crystal diffraction is commonly used as a technique for crystal structure solution and refinement; however, it is increasingly used for more detailed analysis of crystal-chemical features, including charge-density distribution, recognition of static disorder, analysis of temperature and pressure dependence of structure parameters, and many others.

Some of these studies, particularly those involved with highly accurate measurements of electron-density distribution and of displacement parameters, are in need of superior quality diffraction data, as free as possible of random and systematic experimental biases.

In fact, the capability to accurately evaluate experimental single-crystal diffraction intensities plays a crucial role in performing highly reliable refinements when subtle crystal-chemical effects are investigated, such as those that are detectable by means of a proper analysis of atomic displacement parameters *versus* temperature (Pavese, Artioli & Prencipe, 1995; Geiger, Armbruster, Lager, Jiang, Lottermoser & Amthauer, 1992). Furthermore, any study on crystal electrostatic properties involves nonspherical electron-density contributions, which are sensitive to small variations of $|F_{obs}|^2$. Difference electron-density studies also require accurate experimental data, since modest uncertainties in the integrated intensities may degrade the resolution and obscure fine electronic features.

Several experimental biases may occur and affect measured intensities, as well as pure physical effects, such as multiple diffraction (Cole, Chambers & Dunn, 1962; Prager, 1971; Rossmanith, Kumpat & Schultz, 1990; Rossmanith & Kai, 1995) and thermal diffuse scattering (Willis, 1970), which are not easily accounted for.

Common and widely recognized experimental sources of error in the integrated intensities are, for instance, those caused by scan truncation and incorrect estimation of the instrumental background. Scan truncation, in particular, may be a serious problem since it does not allow one to encompass the whole angular range of the peak: broad scans are in competition with scan time and with the necessity of avoiding superpositions between the tails of neighbouring reflections. Most published data are indeed affected by an appreciable amount of tail truncation, yielding: (i) overestimation of the background; (ii) intensity loss, which has been discussed in the literature (Denne, 1977; Destro & Marsh, 1987; Destro, 1988; Suortti, 1994) and, according to the second paper, may be up to 15% of the integrated intensity value. Moreover, the counting noise and signal oscillations may also drastically degrade the quality of data collected, in particular for crystals bearing weak scattering atoms.

Many of these effects are, in principle, detectable through a proper analysis of the intensity profile, which enables experimental data to be partially recovered, provided that a reliable profile model is available.

Although the necessity of accounting for these effects has long been discussed in the literature, most of the commonly used software programs for diffraction data collection and analysis, included those supplied with laboratory X-ray diffractometers, do not provide sufficient analysis and treatment of measured diffraction profiles as they are based on simple numerical sums of the channel

© 1996 International Union of Crystallography
Printed in Great Britain – all rights reserved

counts and neither account for scan-truncation errors nor employ a physically sound model to interpret and check the reliability of experimental data by profile analysis.

Alexander & Smith (1962) pioneered the modelling of the single-crystal diffraction intensity profile, described as the folding of a number of functions representing the contribution of instrumental and crystal effects, though they treated only the case of no monochromatization other than that provided by β filters. Hereafter, we refer to this paper as AS and adopt, in the discussion below, the same formalism. Ladell & Spielberg (1966) improved the previous modelling of AS by developing a treatement to rigorously take into account the effects of the monochromator on the intensity profile.

Further analytical corrections were proposed to account for several single-crystal data-collection effects (Young, 1969; Kheiker, 1969) affecting profiles.

Diamond (1969) first suggested a link between the analysis of single-crystal diffraction intensity profiles and a profile-fitting treatment; he pointed out how 'a suitable curve fitting procedure can reduce the standard deviation of intensity measurements made with a scanning diffractometer'.

Lehmann & Larsen (1974) and Blessing, Coppens & Becker (1974) were concerned with accurate and thorough analyses of step-scanned profiles in order to locate the extremes of the peak region and, consequently, to attain a reliable estimate of the background and of the peak position.

Denne (1977) investigated the effects due to the scan truncation and proposed a correction formula; he maintains, in his paper, that the thermal parameters of several high-temperature structures are affected by serious errors as a consequence of neglecting the scan-truncation effects.

Clegg (1981) presented an on-line implementation of the technique of Diamond, quoted above; Oatley & French (1982) proposed a profile-fitting treatment based on a Bayesian approach to improve the accuracy of the estimation of the integrated intensities.

Destro & Marsh (1987), hereafter indicated as DM, published a paper dealing with the experimental determination of reliable structure factors; they accounted for the intensity loss owing to scan truncation by developing a Fourier-transform-based correction method in the framework of the convolution techniques. Moreover, they remarked on the extreme importance of a reliable background estimate, which they experimentally determined either by performing measurements far from any reciprocal-lattice point or by averaging the counts at the extremes of an expanded scan range around a weak reflection. A further application of the method of DM to account for scan-truncation losses is reported by Destro (1988) in the treatment of low-temperature measurements. In a subsequent paper, Destro & Marsh (1993) extended and improved some aspects of the method they previously presented.

A fairly complete review on data-reduction techniques and error analysis for single-crystal diffraction data was presented by Blessing (1987).

In the present paper, we propose a treatment for single-crystal diffraction intensity profiles based on a profile-fitting technique; the intensity profile is modelled by means of a proper profile function, fully defined by a number of parameters that are refined for each profile and account for the physical effects of diffraction. Such an approach allows one: (i) to extract the integrated intensities by means of a well defined model, which enables separation and treatment of the instrumental contribution to the experimental information; (ii) to recover most of the diffracted intensity lost by scan truncation; (iii) to assess the quality of the measured reflections, discarding those that do not prove to be reliable enough; (iv) to retrieve a number of reflections affected by local biases, detectable as profile anomalies.

Therefore, if the experimental data treated by this method are employed in a structure refinement, we expect (i) an improvement in R factors and, consequently, in the reliability of the experimental structure factors; (ii) a reduction in e.s.d.s of the refined parameters and, hence, a better resolution; (iii) a more realistic estimate of the thermal parameters and of the electron-density population coefficients; (iv) a reduction of noise in difference electron-density maps, which enables a better characterization of the bonding features.

2. Method

2.1. *Model*

As pointed out by AS and DM, the experimental single-crystal intensity profile may be described through the convolution of a number of functions, each accounting for a particular physical effect. Following AS, we model the experimental profile as

$$P(\alpha) = I_\lambda * I_s * I_m * I_x, \qquad (1)$$

where α is the ω angle for an $\omega/2\theta$ scan, I_λ represents the wavelength dispersion function of the radiation employed, I_s accounts for the sample size effect, I_m is due to the mosaicity of the crystal and I_x corresponds to the source effect; $*$ is the symbol of folding.

I_λ is commonly modelled through a Cauchy-like function (AS; Denne, 1977; DM) with the form

$$I_\lambda(\beta) \propto 1/(1 + 2\beta/W^2) \qquad (2)$$

and

$$W = (\Delta\lambda/\lambda)\tan(\theta), \qquad (3)$$

where β is the displacement angle with respect to the Bragg peak position and $\Delta\lambda$ depends on the energy band pass of the monochromator. Formula (2) is a mathematically convenient approximation of the rigorous expression derived by Ladell & Spielberg (1966).

The mosaicity of the crystal is taken into account by the Gaussian function (AS)

$$I_m \propto \exp(-\zeta\beta^2), \quad (4)$$

where ζ is an appropriate coefficient, which should be experimentally determined.

According to AS, the size function I_s is analytically defined by the expression

$$I_s \propto \{1 - [(R/r)\beta]^2\}^{1/2}, \quad (5)$$

where R is the distance between the source and the crystal and r is the linear size of the sample. Since (5) holds for $|\beta| \leq r/R$, corresponding to a very narrow interval, it may be Taylor expanded as a function of β and a second-order truncation shows that this expression can be safely replaced by a Gaussian function.

The I_x function represents the source and there is, at present, no rigorous expression for it; AS employ a trapezoidal function to model the source effect in the case of X-rays, basing their approximation on the observed focal spot of high-quality tubes. I_x mainly depends on the energy distribution in the focal spot and on the collimation of the beam. We expect it to cause the intensity profile to be asymmetric.

As stated above, all functions that are folded together in order to model the observed intensity profiles are represented, or may be replaced, by proper Gaussian or Lorentzian functions. It is well known that, by the associative and commutative properties of the convolutions, the folding of a number of Gaussian and Lorentzian functions, in any order, produces a Voigt function and, hence, the intensity profile function $P(\alpha)$ is a Voigt-like function, apart from source-effect contributions, which are discussed below.

Asymmetry, owing to source effects (such as nonhomogeneous energy distribution in the incident beam) and to the sample (non-ideal lattice), is accounted for by multiplying the theoretical profile function by an empirical function $s(\beta)$, shaped as

$$s(\beta) = [1 - f(\beta)], \quad (6)$$

where $f(\beta)$ is an antisymmetric function [*i.e.* $f(\beta) = -f(-\beta)$], so that

$$\int_{-a}^{+a} m(\beta)\,\mathrm{d}\beta = \int_{-a}^{+a} m(\beta)s(\beta)\,\mathrm{d}\beta \quad (7)$$

if $m(\beta)$ is a generic symmetric function; (7) proves that (6) does not affect the area of the peak, corresponding to the integrated intensity, but only modifies the shape of the profile. Since $s(\beta)$ is strictly empirical, we have asymmetrized the theoretical intensity profile by a simple function, similar to the one adopted by Malmrøs & Thomas (1977), namely,

$$s(\beta) = 1.0 - \beta^2\,\mathrm{sgn}(\beta)\,\nu, \quad (8)$$

where ν is the asymmetry coefficient.

Finally, within 1% error, the Voigt function may be replaced by a pseudo-Voigt function (Young & Wiles, 1988), allowing a simpler parametrization.

On the basis of the discussion above, the intensity profile is modelled by the following function:

$$\begin{aligned} P(\alpha) = I_0\{&[G(\alpha,\alpha_1,\Delta_1)(1-\eta_1) \\ &+ L(\alpha,\alpha_1,\Delta_1)\eta_1]s(\alpha,\alpha_1,\nu_1) \\ &+ k[G(\alpha,\alpha_2,\Delta_2)(1-\eta_2) \\ &+ L(\alpha,\alpha_2,\Delta_2)\eta_2]s(\alpha,\alpha_2,\nu_2)\} + \mathrm{back}(\alpha), \end{aligned} \quad (9)$$

where two pV (pseudo-Voigt) functions are utilized to account for the wavelength doublet ($K\alpha_1$, $K\alpha_2$) when it is necessary. α bears the same meaning as in (1), α_1 and α_2 are the barycenters of the theoretical peaks, k is a factor weighting the contribution of the minor term of the doublet ($K\alpha_2$) with respect to the major one ($K\alpha_1$), η_1 and η_2 distribute the Gaussian and Lorentzian components over each pseudo-Voigt function, ν_1 and ν_2 are the coefficients of the asymmetry functions, Δ_1 and Δ_2 are the full widths at half-maximum. Since each pV function is normalized to unit integral, I_0 corresponds to the scale that, properly corrected by geometrical and polarization factor, yields a quantity proportional to $|F_{\rm obs}|^2$. Finally, back(α) is a generic function representing the background contribution.

A large number of tests have been performed on synthetic profiles in order to check the sensitivity of each parameter of the model function during the refinement. The pV function is flexible enough to allow proper treatment of diffraction data collected with different sources, including X-rays and neutron sources.

The code *PROF*4, which allows treatment of single-crystal diffraction profiles through the model discussed above, has been implemented on-line.

2.2. *Background and k determination*

The reliable determination of the background is a crucial stage for a correct application of the method discussed above. In principle, the background may be modelled through a proper function of the scattering angle having a number of parameters varied during the fitting procedure. Such an approach has proved to be suitable when the background is well defined (*i.e.* when the peak width is much narrower than the scan width). However, a strong background-scale correlation, which drastically affects the results, arises if the background is overestimated (for instance, because of the scan truncation) and consequently the scale factor suffers

from underestimation. To avoid this problem, we have modelled the experimental background by a polynomial function, parametrized *versus* θ (DM). Background values are measured far from any reciprocal-lattice point at several θ positions in order to span the same angular range used in the data collection. A polynomial function is fitted to the measured background values and, subsequently, employed to calculate the background for each intensity profile. Since the background is parametrized only *versus* θ, a number of tests have been performed in order to exclude any significant dependence on the other angles of the diffractometer.

The determination of the k coefficient of (9) is required if the radiation is composed by an emission doublet. In principle, k is very close to 0.5; however, since it depends on many complex experimental variables, such as the setting of the monochromator and the quality of the tube, which may change in time, it is safer to redetermine its value for every data collection.

In general, the k term can be refined by using a number of diffraction profiles of a crystal exhibiting appreciably intense high-angle reflections.

2.3. *Diagnosis of anomalous profiles and 'two steps' retrieval of correct intensities*

One of the attractive aspects of the method consists of its power to retrieve correctly the intensity information yielded by a number of reflections that proved to be strongly affected by instrumental and sample effects. The proposed technique mainly discriminates the estimated intensities on the basis of the angular dependence of the profile FWHM. The FWHM is a parameter that depends on the instrument and on the quality of the crystal. In the ideal case, a slight increase of the FWHM with the θ angle is expected and the intensity profiles that significantly deviate from that trend are tagged as being somehow affected by spurious instrumental or sample effects. The procedure we have developed is as follows:

(i) Firstly, each intensity profile undergoes separate fitting treatment, with independent refinement of all profile parameters, except the k term and background, which are evaluated separately. Full convergence is achieved for a number of reflections, showing figures of merit (see the next paragraph for details) within the selected tolerance range; the rejected reflections do not achieve convergence because of the biases discussed below.

(ii) The FWHM values of the accepted reflections are then plotted *versus* the θ angle; some of their values are spread out, while most of the points follow a well defined trend. These points are used to derive, by least-squares fitting, the actual FWHM function. These reflections are called 'ideal reflections'.

(iii) The discarded reflections commonly show a poorly characterized profile (convergence, when achieved, is merely a numerical artefact, yielding unphysical scale factor and peak width) or a very anomalous profile, revealing the presence of spurious effects, such as multiple diffraction. These reflections are then re-processed using a limited number of profile degrees of freedom, since the FWHM is now calculated by the analytical function developed before (point ii), in order to constrain the profile shape. Convergence is now achieved for a large part of these reflections and the information extracted corresponds to the effective diffraction contribution, according to the profile model.

Moreover, such a technique has proved effective in recovering a number of low-intensity observed reflections, which would be lost if based on counting statistics alone, and this yields a significant improvement of the data-set quality, particularly for weakly scattering crystals.

3. Application and results

A couple of applications of the method discussed above are presented and refer to the treatment of X-ray diffraction data collected on a single crystal of natrolite and to a set of neutron diffraction data collected on a single crystal of pyrope garnet. These two examples are representative of 'difficult' data sets as the former is deeply affected by multiple scattering effects and the latter by scan truncation.

The figures of merit used in the discussion are defined as follows:

$$R_{pw} = \left[(1/n)\sum_{j}^{n}(I_{j,\mathrm{obs}} - I_{j,\mathrm{calc}})^2 \times w_j\right]^{1/2}, \quad (10)$$

where $I_{j,\mathrm{obs}}$, $I_{j,\mathrm{calc}}$ refer to the jth observed and calculated points of the profile, respectively, and w_j is the corresponding weight, defined as $1/I_j$;

$$R = \sum |F_{jc} - F_{jo}| \Big/ \sum |F_{jo}|; \quad (11)$$

and

$$R_w = \left[\left(\sum |F_{jc} - F_{jo}|^2 \times W_j\right) \Big/ \left(\sum |F_{jo}|^2 \times W_j\right)\right]^{1/2}, \quad (12)$$

where F_{jo} and F_{jc} are the jth observed and calculated structure factors, respectively, and W_j the corresponding weight, as $1/(\sigma|F_{jo}|^2)^2$.

The refinements have been carried out by means of a modified version of the *UPALS* code, originally from the University of Uppsala (Lundgren, 1982).

3.1. *X-ray diffraction set: natrolite*

Natrolite is a natural zeolite of chemical formula $Na_2Al_2Si_3O_{10} \cdot 2H_2O$, space group *Fdd2*, D_x = 2.25 g cm^{-3}, Z = 8, a = 18.288 (1), b = 18.644 (1), c = 6.5831 (4) Å. The single crystal employed in the

room-temperature X-ray data collection is a fragment of the same large crystal used for single-crystal low-temperature neutron diffraction (Artioli, Smith & Kvick, 1984). The fragment has been rounded to a near-sphere by the use of a chamber with abrasive walls, in which the crystal is kept in a random motion by an air flux. The minimum and maximum sizes of the ellipsoid are 0.102 and 0.115 mm, respectively. The small and nearly spherical dimensions of the crystal are thought to effectively minimize X-ray absorption effects. 6500 independent reflections ($\pm h, +k, +l$) have been measured in $\omega/2\theta$ scan mode using Mo $K\alpha$ radiation. The angular scan range for each reflection has been determined according to the expression $\Delta\omega = 2.2 + 0.35\tan(\theta)$. The measurements have been carried out on a KUMA-KM4 diffractometer in κ geometry.

The background was previously determined by measurements away from reciprocal-lattice points and, subsequently, parametrized *versus* $\sin(\theta)$ by least-squares fitting of an eight-order polynomial function, $B(\theta)$.

The k term of (9) has been refined [$k = 0.47$ (5)] using 22 high-angle intensity profiles, whose backgrounds were estimated by means of $B(\theta)$.

Since the diffraction profiles exhibit a very slight asymmetry that, as tests have proved, does not appreciably affect the scale factor, and the refinement of the asymmetry coefficient is very complex and unstable whenever the effect is minor, ν_1 and ν_2 terms have arbitrarily been fixed at zero; two Gaussian functions are adequate to describe the peaks of the doublet.

$K\alpha_1$ and $K\alpha_2$ peaks have been constrained to be located far from one another according to the theoretical dispersion; only the position of the barycentre of the $K\alpha_1$ peak has been refined. Moreover, such a constraint contributes to highlight multiple diffraction effects and to partially recover the affected reflections. In fact, their profiles are characterized by the presence of spurious peaks, which are not accounted for by the model and therefore only the portion matching the calculated intensity profile and corresponding to the primary diffraction signal effectively contributes to the extracted intensity. Fig. 1 reports the experimental and calculated profiles for a typical peak affected by multiple reflection, as confirmed by simulation (Rossmanith, Kumpat & Schultz, 1990); in this case, the recovery of the primary diffraction peak has turned out successful as allowed by the net split with respect to the spurious bump.

The $K\alpha_1$ peak location, the widths of the doublet peaks and the scale have been refined for each reflection.

In Fig. 2 are reported the breadths of all profiles for which $R_{pw} \leq 0.03$. The 'ideal reflections' subset includes only those reflections having FWHMs in the range 0.1–0.3°. On the basis of this partial reflection set, we have parametrized the FWHM as a function of θ.

Structure refinements started from the atomic parameters reported by Artioli, Smith & Kvick (1984). Coordinates, atomic displacement parameters and scale factor were allowed to vary, apart from the atomic parameters of the H atoms, according to the symmetry constraints; atomic scattering factors for neutral atoms were taken from *International Tables for Crystallography* (1992); the intensities have been corrected for absorption and those reflections showing an $|F_o|/|F_c|$ ratio ≥ 2.5 have been discarded during the refinement; only $I \geq 3\sigma$ data have been considered. The imposed cut-off boundaries result in a slightly different number of reflections in each refinement.

We have adopted the simplest weighting scheme, namely $1/\sigma^2$. In general, each reflection may be weighted on the basis of σ, estimated either through

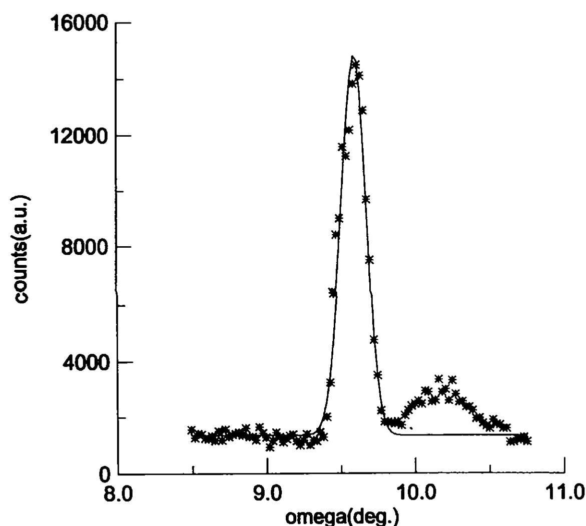

Fig. 1. Experimental (symbols) and calculated (solid line) profiles of the 840 reflection of natrolite affected by multiple diffraction.

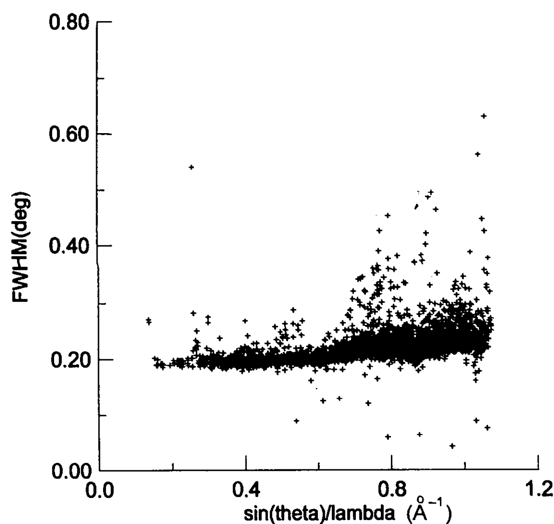

Fig. 2. FWHM of $K\alpha_1$ peaks; data refer to natrolite.

the classic calculation or as the error of the scale factor from profile fitting. In the first case, the error is entirely attributed to the uncertainty in counting, whereas, in the second case, the weight indicates the match of the model profile. In this case, the statistical oscillations indirectly influence the error of the individual intensities.

Figs. 3(*a*) and (*b*) report on the same scale the weights, normalized to unity, attained by the classical (W_c) and the present (W_p) method. W_c and W_p show rather different trends; in the first case, the weights decrease for high-angle reflections, whereas for W_p the points are gathered around a mean value, apart from a number of spread out reflections that bear large weights,

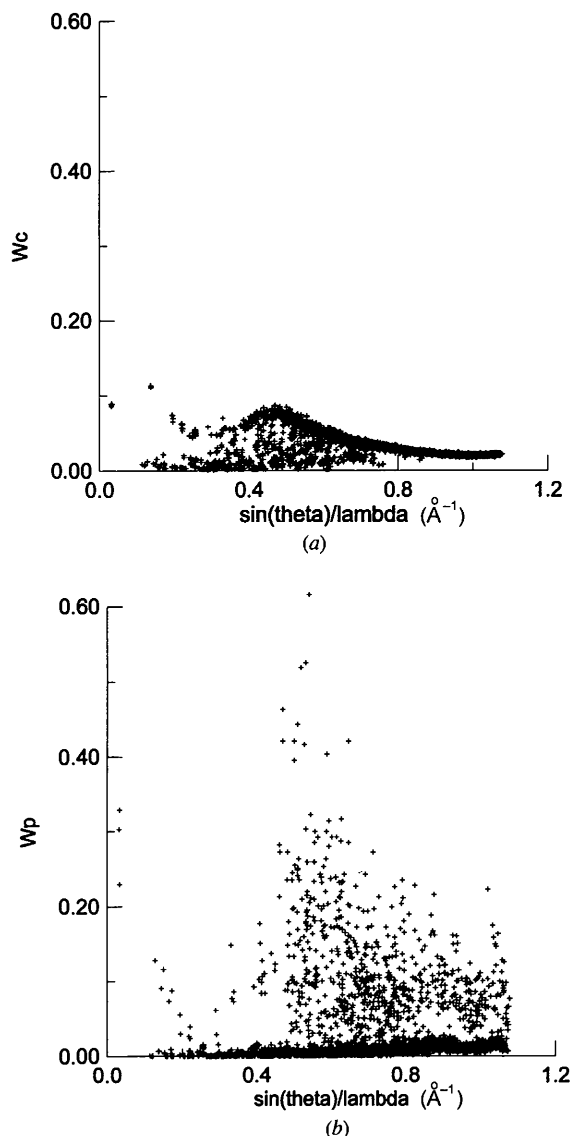

Fig. 3. Weights normalized to unity; they are calculated (*a*) by the classical approach and (*b*) through the profile-fitting treatment. Data refer to natrolite.

since their theoretical profiles fit very well to the experimental ones. Table 1 shows the results of the refinements.

Rows 1–5 in Table 1 report the results of the refinements obtained by selecting those reflections such that $R_{pw} \leq 0.03$, regardless of the value of the FWHM. A comparison of rows 1 and 4 reveals that the data treated by profile fitting (p.f.) lead to a substantially better R factor, with respect to that resulting from conventionally integrated (c.i.) data; R_w factors cannot be directly compared since different weighting schemes are adopted. In the case of p.f. data, the ratios σ/x and σ/U show an improvement and, moreover, a larger number of reflections fall in the selected tolerance range. Comparison of rows 2 and 4, wherein the same weighting scheme has been used, shows that the R_w of the p.f. $|F_{\rm obs}|^2$ turns out to be better than that of the c.i. data. At a first glance, it seems that the resolution on the atomic displacement parameters favours the c.i. data, but it is necessary to take into account the larger number of variables averaged to calculate the σ/U ratio in the case of the p.f. set. Rows 6 and 7 report the results attained from 'ideal reflections' and from the data set obtained adding the retrieved reflections to the ideal ones, respectively. Although R of row 7 worsens, compared with that of row 6, however, the number of reflections in the refinement, and the anistropic displacement parameters (a.d.p.) such that $U \geq 3\sigma$, increases, and the σ/x mean ratio diminishes. The increased R factor reflects the fact that the retrieved reflections are degraded with respect to the ideal ones, although, taking into account that they are properly weighted, they significantly contribute to further constrain the model and the results are more reliable in terms of the refined σ's. A comparison of rows 9 and 8 proves that the profile-fitting method allows extraction of $|F_{\rm obs}|^2$ that better match the $|F_{\rm calc}|^2$ values on the basis of the standard diffraction theory and provides an improvement to the resolution of coordinates and atomic displacement parameters.

The following points deserve to be highlighted:

(i) The R factor is systematically lower for p.f. than for c.i. data sets. This usually implies an improvement in determining electronic features. R_w behaves like R for comparable data sets.

(ii) σ/U and σ/x ratios are smaller for p.f. data.

(iii) The number of reflections accepted in the refinements is larger for p.f. data.

(iv) The number of refined U variables, such that $U > 3\sigma$, is systematically larger for p.f. data.

3.2. *Neutron diffraction set: pyrope garnet*

The general chemical formula of garnets ($Ia\bar{3}d$, $Z = 8$, $D = 3.58\,{\rm g\,cm^{-3}}$) is $X_3Y_2Z_3O_{12}$, where X (Mg, Fe, Mn, Ca), Y (Al, Fe) and Z (Si) are eight-, six- and four-coordinated sites, respectively; in the case of pyrope [$a = 11.459\,(4)$ Å], X is occupied by Mg and Y by Al.

Table 1. *Refinement results for natrolite*

The first column lists the data-set number; the string of characters codes the kind of data set employed, as follows: P = profile-fitting-treated data, C = classically treated data, p means weight from profile fitting technique, $p = c$ means weight from the classical approach, $p = 1$ means unit weight, x means that no cut-off boundary is used on FWHM to select reflections, l means that only those reflections having a FWHM within a chosen range have been considered; r indicates that the calculation has been performed on a data set obtained by joining the data of the previous l set with the retrieved reflections, as explained in the text. Results characterized by the same code refer to the same *hkl* set, with different $|F_o|^2$ and $\sigma(|F_o|^2)$, according to the integration scheme. Figures of merit are described in the text; σ/x and σ/U correspond to the mean values of the ratios e.s.d./coordinate and e.s.d./a.d.p.; only those variables with values larger than 3σ are taken into account and the associated integer represents the number of refined variables satisfying this constraint. N is the number of reflections such that $|F_o|/|F_c| \leq 2.5$ and $|F_o|^2 \geq 3\sigma(|F_o|^2)$, namely those actually used in the refinement.

	Data type			$R \times 100$	$R_w \times 100$	N	σ/x		σ/U	
1	P	p	x	2.664	2.982	1590	0.00089	27	0.093	47
2	P	p=c	x	2.786	2.734	1564	0.00098	27	0.119	47
3	P	p=1	x	2.625		1564	0.00109	27	0.112	47
4	C	p=c	x	2.922	3.139	1499	0.00117	27	0.108	42
5	C	p=1	x	2.832		1499	0.00125	27	0.096	41
6	P	p	l	2.194	2.759	1491	0.00094	27	0.095	41
7	P	p	r	2.722	3.609	1835	0.00078	27	0.093	49
8	P	p=c	r	2.517	2.459	1690	0.00081	27	0.094	46
9	C	p=c	r	3.172	4.337	1625	0.00147	27	0.123	40

Two data collections at room temperature have been performed at the BNL HFBR reactor, employing a natural single crystal of pyrope, as a cube with 0.5 cm edge length. We have selected the data sets as examples of high-quality neutron diffraction data. In the following discussion, we have artificially truncated by about 15% on each side the measured scan range of the data set collected with the pyrope crystal enclosed in a temperature mirror furnace, subsequently used for high-temperature data collections up to 1100 K. This data set represents well the kind of data available when the experimental background is affected by instrumental contributions (powder lines of Al, Ti, Al_2O_3 from the furnace materials) and possibly affected by scan truncation, often caused by limited time allocation at neutron sources. The refinement performed on this artificially 'worsened' data set is compared with the one performed on the data set measured at room temperature with the same pyrope crystal on the same instrument with no furnace in the beam, using the full scan profiles and adopting the classic integration scheme to extract the intensities.

Nearly 1200 reflections have been measured in $\omega/2\theta$ scan mode for each of the two data sets. The angular scan range has been chosen according to the expression

$$\Delta(2\theta) = 1.555 + 2.853\tan(\theta), \quad 2\theta \geq 55^\circ$$

$$\Delta 2\theta = 3.0, \quad 2\theta \leq 55^\circ$$

and the measurement time for each reflection has been determined by monitoring the incident beam until a specific number of counts has been reached. A Be monochromator with (002) as reflecting plane was used to obtain a wavelength of λ = 1.0462 Å, calibrated against a KBr lattice constant a = 6.6000 (1) Å at 298 K. Background has been determined as explained in the previous section by measurements in the 5–60° θ range.

Peaks exhibit a Gaussian shape (Fig. 4), with asymmetry nearly absent. The peak position, the FWHM and the scale have been varied for each reflection.

Cordinates, atomic displacement parameters, extinction coefficient (secondary extinction, type I, modelled by a Lorentzian mosaic distribution) and scale factor were allowed to vary, according to the symmetry constraints; reflections such that the ratio $|F_o|/|F_c| \geq 2.5$ have been discarded during the refinement; only $I \geq 3\sigma$ data have been considered. The results reported in Table 2 refer to the reflections (obtained by integration over artificially truncated scan ranges) selected by retaining those that lead to an R_{pw} smaller than 0.03 and have FWHMs oscillating ±0.15° around the value of the main trend.

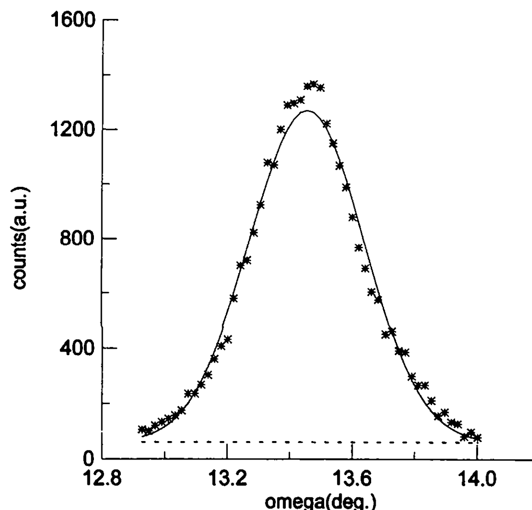

Fig. 4. Experimental (symbols) and calculated (solid line) profiles of the $4\bar{3}1$ reflection of pyrope affected by intensity loss owing to scan truncation; the dashed line represents the background estimated as described in the text.

Table 2. *Refinement results for pyrope garnet*

The results have been obtained by integration over artificially truncated diffraction profiles. Abbreviations are as described in Table 1.

	Data type			$R \times 100$	$R_w \times 100$	N	σ/x	σ/U
1	*P*	*p*	*l*	2.705	2.206	205	0.00108 3	0.139 15
2	*P*	*p*=1	*l*	2.697		206	0.00105 3	0.110 15
3	*P*	*p*=*c*	*l*	2.769	1.694	208	0.00102 3	0.131 15
4	*C*	*p*=*c*	*l*	3.238	1.771	210	0.00110 3	0.087 15
5	*C*	*p*=1	*l*	3.159		211	0.00124 3	0.085 15

The experimental intensities have been corrected for sample absorption.

Rows 1 and 4 of Table 2 clearly show that the data treated by the profile technique yield better *R* factors compared with those processed by the simple integration method. Morever, rows 3 and 4, where the same weighting scheme is used, prove that the R_w factor slightly decreases for the p.f. data set as well. Finally, rows 2 and 5, where unit weights have been adopted, indicate that the $|F_c|^2$ better match the p.f. than the c.i. observed intensities. In the present case, the number of retrieved reflections is rather modest (15) and, consequently, no further improvement results from their introduction; this confirms the good quality of the counting statistics of these experimental data.

The atomic displacement parameters determined by the c.i. data set turn out to be 76% larger with respect to those from data treated through the profile-fitting method. This result is expected as the scan truncation affecting the intensity profiles leads to a serious underestimation of the net intensity of each reflection; with the assumption that the structural degrees of freedom are limited to the oxygen coordinates, this lack of intensity entirely reflects on the a.d.p., increasing them to lower F_c values. Moreover, the better resolution on a.d.p. resulting from the c.i. data set is simply a consequence of the abnormally high value of the thermal parameters, which decreases the σ/U ratio.

A comparison of the a.d.p. obtained from p.f. and c.i. data with respect to those derived from data collected outside the furnace and not affected by scan truncation (reference data) reveals 12 and 67% mean overestimations, respectively. This confirms that the proposed method has successfully improved the quality of experimental integrated intensities of biased diffraction profiles; the deviations still remaining between p.f. and reference data may be due to the absorption effects of the conditioning chamber not being entirely accounted for.

The authors thank G. Ferraris for useful comments and discussions, and the referees for suggestions to improve the manuscript. Neutron scattering data are from a wider data set collected at HFBR, Brookhaven National Laboratory (USA) with the help of R. K. McMullan; a full report of this project will be published elesewhere. The present research has been funded by Italian CNR and MURST funds.

References

Alexander, K. E. & Smith, G. S. (1962). *Acta Cryst.* **15**, 983–1004.

Artioli, G., Smith, J. V. & Kvick, Å. (1984). *Acta Cryst.* C**40**, 1658–1662.

Blessing, R. H. (1987). *Crystallogr. Rev.* **1**, 3–58.

Blessing, R. H., Coppens, P. & Becker, P. (1974). *J. Appl. Cryst.* **7**, 488–492.

Clegg, W. (1981). *Acta Cryst.* A**37**, 22–28.

Cole, H., Chambers, F. W. & Dunn, H. M. (1962). *Acta Cryst.* **15**, 138–144.

Denne, W. A. (1977). *Acta Cryst.* A**33**, 438–440.

Destro, R. (1988). *Aust. J. Phys.* **41**, 503–510.

Destro, R. & Marsh, R. E. (1987). *Acta Cryst.* A**43**, 711–718.

Destro, R. & Marsh, R. E. (1993). *Acta Cryst.* A**49**, 183–190.

Diamond, R. (1969). *Acta Cryst.* A**25**, 43–55.

Geiger, C. A., Armbruster, T., Lager, G. A., Jiang, K., Lottermoser, W. & Amthauer, G. (1992) *Phys. Chem. Miner.* **19**, 121–126.

International Tables for Crystallography (1992). Vol. C. Dordrecht/Boston/London: Kluwer Academic Publishers.

Kheiker, D. M. (1969). *Acta Cryst.* A**25**, 82–88.

Ladell, J. & Spielberg, N. (1966). *Acta Cryst.* **21**, 103–122.

Lehmann, M. S. & Larsen, F. K. (1974). *Acta Cryst.* A**30**, 580–584.

Lundgren, J.-O. (1982). *UPALS Crystallographic Computer Programs*. Report UUIC-B13-4-05, University of Uppsala, Sweden.

Malmrøs, G. & Thomas, J. O. (1977). *J. Appl. Cryst.* **10**, 7–11.

Oatley, S. & French, S. (1982). *Acta Cryst.* A**38**, 537–549.

Pavese, A., Artioli, G. & Prencipe, M. (1995). *Am. Mineral.* **80**, 457–464.

Prager, P. R. (1971). *Acta Cryst.* A**27**, 563–569.

Rossmanith, E. & Kai, B. (1995). *Acta Cryst.* A**51**, 134–142.

Rossmanith, E., Kumpat, G. & Schultz, A. (1990). *J. Appl. Cryst.* **23**, 99–104.

Suortti, P. (1994). *Mater. Sci. Forum*, **166/169**, 213–232.

Willis, B. T. M. (1970). Editor. *Thermal Neutron Diffraction.* Oxford University Press.

Young, R. A. (1969). *Acta Cryst.* A**25**, 55–66.

Young, R. A. & Wiles, D. B. (1982). *J. Appl. Cryst.* **15**, 430–438.